Photon drag investigations of current relaxation processes in a two-dimensional electron gas

S. Graf and H. Sigg
Paul Scherrer Institute, Laboratory for Micro- and Nanotechnology, CH-5232 Villigen-PSI, Switzerland

K. Köhler
Fraunhofer Institut für Angewandte Festkörperphysik, Tullastrasse 72, D-79108 Freiburg, Germany

W. Bächtold
Laboratory for Electromagnetic Fields and Microwave Electronics, ETHZ, CH-8092 Zürich, Switzerland
(Received 21 March 2000)

We have investigated the photon drag current that is excited by an infrared laser beam in the plane of the two-dimensional electron gas of $GaAs/Al_{0.35}Ga_{0.65}As$ multiple-quantum-well systems. An analysis of the spectral response, measured with the picosecond infrared pulses of the wavelength-tunable free electron laser source FELIX, is presented for different doping schemes and examined as a function of temperature and intensity. The influence of the subband-selective scattering by a δ doping is explored, which demonstrates that the photon drag spectral response allows the determination of the momentum relaxation time ratio, $R = \tau_1/\tau_2$, of the electrons in the ground and excited subbands. The relaxation time ratio is found to be surprisingly constant over a large temperature range. The variation of the ratio with intensity can be attributed to heating of the electron gas, whose temperature exceeds 1000 K at saturation intensity.

I. INTRODUCTION

The photon drag (PD) effect is the generation of an electrical current in a solid by the momentum transfer from absorbed photons. The classical appearance as radiation pressure on a surface was described already in 1861 by Maxwell. The first PD generated by optical transitions between subbands in *p*-Ge was investigated independently by two groups, Gibson *et al.*[1] and Danishevskii *et al.*[2]

With the realization of the intersubband absorption in quantum-well (QW) systems,[3] a large increase in sensitivity was achieved, related to the resonant interaction in an intersubband transition with its intrinsically large absorption coefficient. Moreover, new features of the PD in two-dimensional electron gases (2DEG's) were predicted by Luryi[4] and Grinberg and Luryi[5] and observed experimentally by Wieck *et al.*[6] These features occur as a result of the difference in the momentum relaxation rates in the ground and excited subbands and have an interesting analogy in the Doppler-effect-induced drift of atoms, the so-called light-induced drift.[7,8]

The many fascinating aspects of the effect came only into the reach of experiments with the advent of an easily tunable infrared source. The free-electron laser for infrared experiments (FELIX) of the FOM Institute for Plasma Physics in the Netherlands provided the infrared light for the experiments of Sigg *et al.*,[9–11] as well as for the measurements presented here. The findings were not only a motivation for further experiments but also inspired several theory groups to contribute and predict new PD phenomena.[12–14] The resolution of peculiar details of the spectral dependence of the PD effect allows us to obtain information on the intersubband and interband relaxation processes. By comparing absorption and PD spectra, the depolarization shift can directly be observed.[15,16]

The intersubband relaxation processes are of fundamental importance for the now widely used QW infrared (ir) devices. Commonly used techniques for their study include the measurement of ir absorption, saturation, pulse pump/probe, and photoconductivity. In general, these all-optical techniques probe energy relaxation times. The PD effect reveals complementary information, since it is a photoelectric effect and is directly linked to the current or momentum relaxation times.

The intention of this paper is to present and discuss new experimental evidence confirming the reliability of the single-electron-based PD model introduced in Sec. II and to discuss the linewidth differences between the spectra obtained in attenuated total reflection and PD experiments. The resonance position differences have been discussed in Refs. 13 and 15. The samples and the experimental setup used are given in Sec. III. We present in Sec. IV the results of our PD experiments. In Sec. IV A, it is shown that the PD effect is sensitive to the subband-dependent relaxation time. In Sec. IV B, the measured signal response is related to the amount of momentum transferred from the photons to the electrons. In Secs. IV C and IV D, we present investigations of the subband relaxation rates as a function of temperature and intensity. We conclude in Sec. V that PD spectroscopy is a versatile tool to investigate the dynamics of intersubband transitions.

II. MODEL

The PD effect resulting from an intersubband absorption in a QW system is a current due to momentum transfer to electrons in the excited subband and empty states (in the following, denoted as holes) in the ground subband. It is possible to separate the PD current into two components.

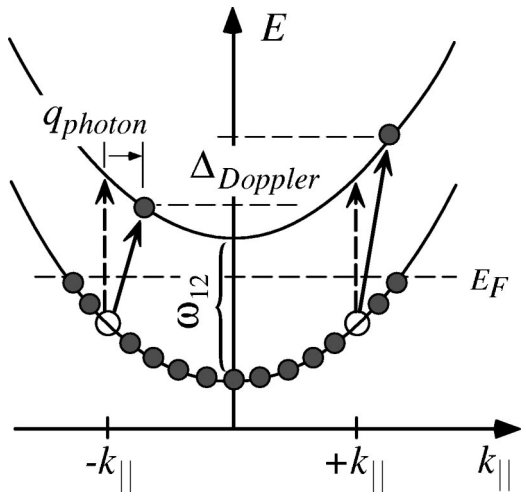

FIG. 1. Energy diagram with the nonvertical transitions between ground and first excited subbands by absorbing ir light with a wave vector $\mathbf{q}_{Photon}$ (for clarity, $\mathbf{q}_{Photon}$ has been greatly enlarged). Depending on the difference between the photon energy and the ISR energy $\hbar\omega-\hbar\omega_{12}$, transitions at negative or positive $k_{\|}$ (with respect to the direction of the light propagation) are excited (Doppler effect).

The so-called direct part of the PD signal is a consequence of the direct momentum transfer from the photon to the electron system and is thus proportional to the absorption and the photon momentum $p=h\nu n/c$, where c is the speed of light and n is the refractive index in the active medium, in our case $n_{\mathrm{GaAs}}=3.28$.

To explain the resonant contribution denoted as the resonant PD current, we have to note that the intersubband transition of an electron leaves a hole in the ground subband. The wave vectors of the excited electrons and holes are determined by the energy and momentum conservation laws. As can be seen in the subband energy diagram of Fig. 1, negative or positive wave vectors k (with respect to the direction of the light propagation) are selected, depending on the energy $\hbar\omega$ of the incident photon. Classically, this selective excitation is described as the Doppler effect. The corresponding shift, $\Delta_{\mathrm{Doppler}}$, is in our intersubband systems less than 1.2 meV (maximum at the Fermi edges, cf. Fig. 1) and is therefore of minor importance for the absorption line profile, whose width is more than 6 meV at room temperature (RT). For the PD effect, however, this small shift is very essential.

Let us consider an intersubband transition occurring at the wave vector $\mathbf{k}$. The thereby generated currents are proportional to $\mathbf{k}$, the charges, and the corresponding relaxation time, τ_1 for the holes in the first subband and τ_2 for the excited electrons in the second subband. Thus the effective momentum transfer occurs in this case between the lattice and the electrons, whereas the photon momentum only determines the selection of $\mathbf{k}$. It should be noted that $\mathbf{k}$ can be two orders of magnitude larger than the photon wave vector $\mathbf{q}=\mathbf{p}/\hbar$, but also that the magnitude of both currents is comparable (for $\tau_1\approx\tau_2$), while the directions are opposite.

Since the absorption lineform is lifetime broadened, all possible individual contributions have to be taken into account to obtain the total resonant PD current, i.e., we have to sum over all k states. In this sum, one has to take into account that due to the Doppler effect, the transition energy for an excitation at any negative k differs from the corresponding transition at positive k by $2\hbar^2\mathbf{k}\cdot\mathbf{q}/m^*$, where m^* is the effective mass of the electron (cf. Fig. 1). In other words, the transition probability for an electron to be absorbed depends on its wave vector. The resulting resonant PD current is thus changing its sign when the energy is swept through the intersubband resonance (ISR). The proper calculation yields a spectral response that is proportional to the derivative of the absorption. This means that the spectrum is antisymmetric with respect to the energy $\hbar\omega_{12}$ of the single-particle excitation at $k=0$.

Finally, the resonant and direct contributions lead to the following frequency dependence of the photon drag effect:[17]

$$i_{PD}\propto\tau_2\left(\alpha(\omega)+\frac{\partial\alpha(\omega)}{\partial\omega}\frac{\langle E\rangle}{\hbar}(\tau_1/\tau_2-1)\right), \tag{1}$$

where $\langle E\rangle$ is the mean value of the electron energy in the ground subband, given by

$$\langle E\rangle\equiv N_{el}^{-1}\int_0^\infty f_{FD}(E)\,g_{2\mathrm{D}}\,E\,dE \tag{2a}$$

with the surface electron density $N_{el}\equiv\int_0^\infty f_{FD}(E)\,g_{2\mathrm{D}}dE$ and the density of states $g_{2\mathrm{D}}=m^*/(\pi\hbar^2)$ of the ground subband, where the Fermi-Dirac distribution is

$$f_{FD}(E)=\frac{1}{\exp[(E-\mu)/k_BT]+1}, \tag{2b}$$

with Boltzmann's constant k_B. The chemical potential μ is obtained from

$$E_F=\mu+k_BT\ln(1+\exp[-\mu/k_BT]). \tag{2c}$$

In particular, at $T=0$ K, we obtain $\langle E\rangle=E_F/2$.

For illustration, we have calculated with Eq. (1) the spectral shape of the PD response, with different ratios of the subband relaxation times τ_1/τ_2, using a Lorentzian type lineform with the linewidth Γ [full width at half maximum (FWHM)]. The distinct difference of the spectral line shapes are visible in Fig. 2 for τ_1/τ_2 equal to 3, 2, 1, 1.5, 0.6, and 0.3, where the ratio $\Gamma/(2\langle E\rangle)$ has been set to 0.3, a typical value in our experiments. At this point we would like to note that Eq. (1) coincides with that obtained in Refs. 4 and 5 in the typical experimental situation of a small Doppler shift, i.e., $|2\hbar^2\mathbf{k}\cdot\mathbf{q}/m^*|\ll\Gamma$.

In the above simple model we have neglected the influence of many-body effects such as the resonant screening of the light (alternatively called the depolarization field), which increases the resonance energy. A theoretical treatment of this problem, employing the self-consistent field method, is given by Załużny.[13] Applying his theory yields a new method to directly observe the depolarization shift. This is realized experimentally by the comparison of an absorption measurement with the photon drag line shape.[15] In the following, we will not distinguish the shifted ($\tilde{E}_{12}$) from the unshifted ($E_{12}\equiv\hbar\omega_{12}$) intersubband transition energy, as it does not affect the general interpretations given in this paper.

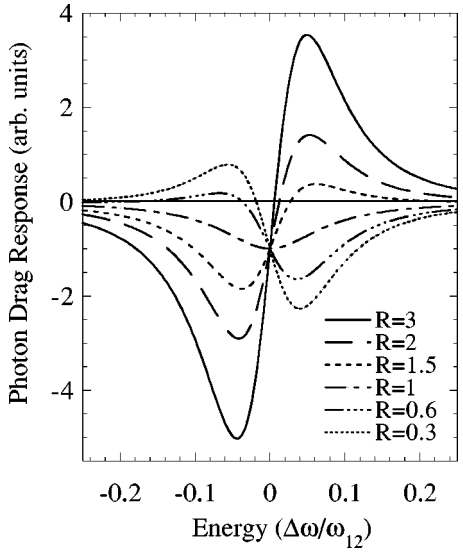

FIG. 2. Calculated PD spectrum for different relaxation time ratios $R=\tau_1/\tau_2=3$, 2, 1, 1.5, 0.6, and 0.3. The ratio $\Gamma/(2\langle E\rangle)$ [cf. Eq. (1) in the text] has been set to 0.3. Not that for $R=1$, the PD coincides with the absorption line form, which is symmetric about the resonance frequency ω_{12}.

III. SAMPLES AND EXPERIMENTAL SETUP

The samples were grown by molecular-beam epitaxy and consist of a 30-period modulation-doped multiple-QW system made of 82-Å GaAs wells and 260-Å $Al_{0.35}Ga_{0.65}As$ barriers, with 0.87×10^{12} cm^{-2} and 0.93×10^{12} cm^{-2} electrons per well for samples A and B respectively. The third sample C, with a δ doping in the center of the well, is a 40-period QW system made of 84-Å GaAs wells and 146-Å $Al_{0.35}Ga_{0.65}As$ barriers, having an electron density of 1.15×10^{12} cm^{-2} per well. The top and bottom layers adjacent to the multiple-QW (MQW) structures were designed to properly compensate for the surface charge and the background doping in the buffer layer and the substrate, respectively. Figure 3 shows diagrams of the energy levels, wave functions, and doping sites of the different samples.

The Fermi energy lies between the first two subbands, and therefore also at RT, a single intersubband absorption at $\sim$120 meV is observed. To provide the optical coupling to the ISR, we took advantage of the attenuated total reflection (ATR) geometry by using a Ge prism pressed onto the QW samples. The frequency dependence of the absorptance (defined as the absorbed fraction of the incident energy), derived from an effective medium approach[18] at the critical angle of incidence, $\varphi_c=\arcsin(n_{\mathrm{GaAs}}/n_{\mathrm{Ge}})$, can be written as

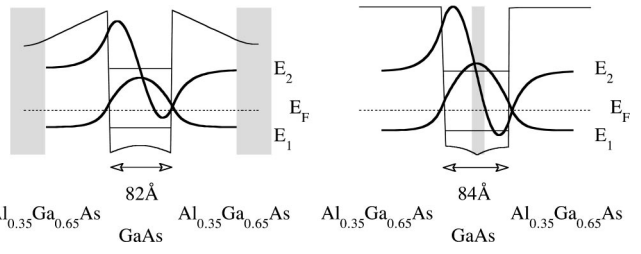

FIG. 3. Diagram of the energy levels, showing wave functions and doping sites of (a) the modulation-doped samples A and B and (b) the δ-doped sample C. The energy spacing between the subband $|1\rangle$ and subband $|2\rangle$ is $\sim$120 meV.

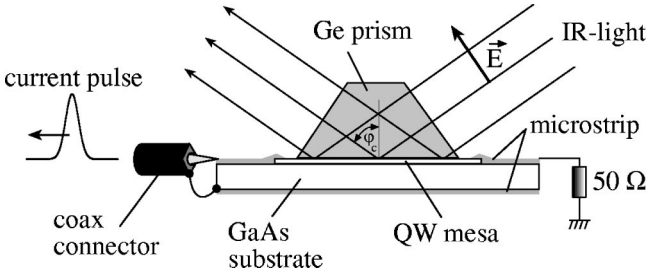

FIG. 4. Schematic structure of the device with the multiple quantum-well mesa formed as a microstrip. The in-coupling of the incident *p*-polarized light to the active 2DEG layer is via the attenuated total reflection (ATR) scheme at the critical angle, $\varphi_c=56°$, of the interface between the Ge prism and the $GaAs/Al_xGa_{1-x}As$ mesa. The generated PD current is coupled via a microstrip line into the 50 Ω coaxial cable.

$$A_{MQW}(\omega,\varphi_c)\simeq 1-\exp\left\{-N_{QW}g_c\frac{N_{el}e^2f_{12}\hbar}{c\sqrt{\varepsilon_{\mathrm{GaAs}}}\varepsilon_0 m^*\Gamma}\times\frac{1}{\{[(E_{12}-\hbar\omega)2/\Gamma]^2+1\}}\right\}, \tag{3}$$

where $f_{12}=2m^*\hbar^{-2}E_{12}z_{12}^2$ is the oscillator strength associated with $1\rightarrow2$ transitions, $\tau=2\hbar/\Gamma$ is the dephasing time, N_{QW} is the number of QW's, e is the charge of the electron, and $\varepsilon_{\mathrm{GaAs}}=n_{\mathrm{GaAs}}^2$. For the geometry factor, we obtain $g_c=4\varepsilon_{\mathrm{GaAs}}^{3/2}n_{\mathrm{Ge}}/[\cos(\varphi_c)|\varepsilon_{QW}|^2]$, which is close to the value used in the traveling-wave equation given by Załużny and Nalewajko.[19] The validity of Eq. (3) was confirmed by experiments on a 10 QW structure with the same well and barrier dimensions as in sample A and with an electron density of 0.76×10^{12} cm^{-2} per well. The absorptance with a FWHM of 7 meV had a maximum of 0.9, which agrees very well with the estimation. This experiment also illustrates that the prism coupling used in the ATR scheme is highly efficient, since for the same absorptance, one would need at least 9 consecutive passes through the 10 QW layers in the commonly used 45° waveguide geometry.[20]

The signal detection scheme, shown in Fig. 4, relies on the integration of the active QW layer into a microstrip, forming a microwave transmission line.[9,10,21] As described above, the incoupling of the light is accomplished using a Ge prism placed on top of the sensitive area.[22] The microstrip arrangement with total reflection incoupling provides some important experimental advantages. First, at the critical total reflection angle, the electric field of *p*-polarized light is exactly perpendicular to the quantum layers, providing optimal coupling to the ISR. Second, due to the illumination through the surface, the far-infrared field strength is constant along the propagation direction of the light, which avoids (electron) temperature gradient-induced currents. Third, measurements of the signal transients are possible over a bandwidth that exceeds 30 GHz. This is essential for the high-frequency (HF) measurements, when working with pulsed ir sources, as, for example, the free electron laser FELIX used here. FELIX produces[23] a train of micropulses at 1-ns intervals

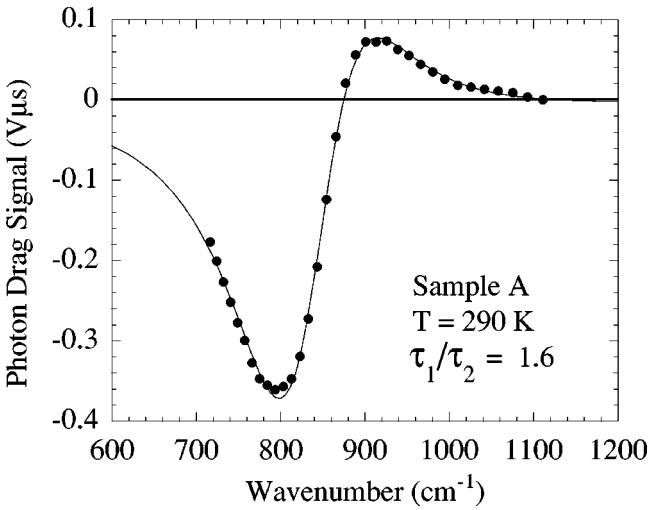

FIG. 5. Photon drag spectrum at RT of the modulation-doped GaAs/Al_xGa_{1-x}As MQW sample A, measured at a micropulse intensity of 2.5 MW/cm^2. For a better signal to noise ratio, an integration is made over the entire macropulse of FELIX (5.6 μs). A Lorentzian absorption is used in the fit (solid line) using Eq. (1). The spectral line shape yields a relaxation time ratio of 1.6.

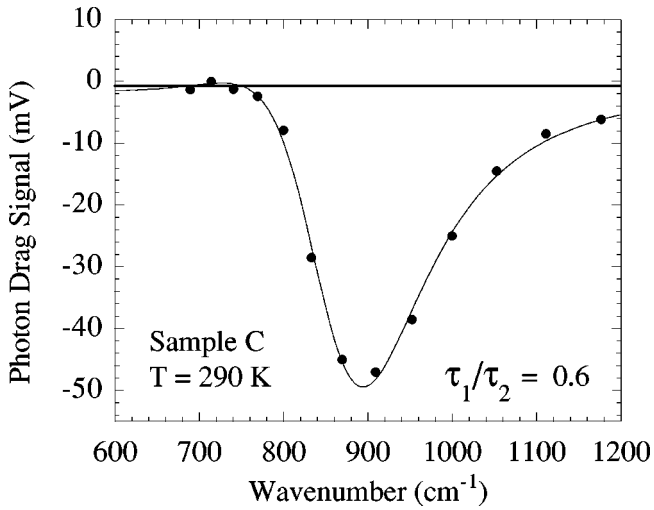

FIG. 6. Photon drag spectrum at RT of sample C (δ doping at the center of the GaAs QW) measured at a micropulse intensity of 3.6 MW/cm^2. The fit of the spectral line shape (solid line) using a Lorentzian absorption in Eq. (1) yields a relaxation time ratio of 0.6. A ratio below 1 indicates that the ground state is more affected by the δ doping than is the first excited. Note the characteristic difference in the line form in comparison with Fig. 5.

during a macropulse of several microseconds. The best signal-to-noise performance is obtained by electrical low-pass filtering of the pulsed PD signal at $\sim$1 MHz, the time scale of the macropulse.

IV. EXPERIMENTAL RESULTS AND DISCUSSION

A. Photon drag spectra

An apparent characteristic of the PD effect is that it probes the ratio $R=\tau_1/\tau_2$ of the relaxation times in the ground and excited subbands [cf. Eq. (1)], and therefore special attention was devoted to systems where this ratio is changed. In Fig. 5, the spectral response of the PD effect in the modulation-doped MQW sample A with an internal intensity of 2.5 MW/cm^2 is presented. The spectral dependence of the PD signal allows the separation of the resonant and direct PD component and thus the determination of the relaxation time ratio. Assuming a Lorentzian line form for $\alpha(\omega)$ in Eq. (1), we find the ratio $R=1.6$. For $\langle E\rangle$ at RT, we obtain 33.8 meV. According to the arguments given by Sigg *et al.*,[11] the maximum value for the momentum time ratio can be assessed from the current relaxation time τ_{Hall}, related to the Hall mobility $\mu_{Hall}=e\tau_{Hall}/m^*$ [μ_{Hall}(300 K)$=$7800 cm^2/V s], as a guess for τ_1, and from the absorption linewidth $\Gamma_{ATR}\simeq 12$ meV obtained with a Fourier transform (FT) spectrometer, which is an estimation for τ_2. Since $T_2=2\hbar\Gamma_{ATR}^{-1}$ also includes phase relaxation processes (e.g., electron-electron scattering) that preserve the total electron momentum, the current relaxation time τ_2 is always larger than T_2. We thus obtain an upper limit $\tau_{Hall}/T_2\simeq 2.7$ for the ratio. A more comprehensive discussion related to the ratio and its estimate will be given below.

The linewidth extracted from the PD spectrum in Fig. 5, using Eq. (1), is rather large: $\Gamma_{PD}\simeq 24$ meV. This is partially due to the high excitation density of 2.5 MW/cm^2, leading to heating of the electron gas, as will be discussed in more detail below. However, at low intensity, the width for the modulation-doped QW is found to remain a factor of 2 larger than Γ_{ATR}. In part this is due to the time structure of FELIX (4.8 ps correspond to a spectral width of 0.4 meV) and in part to optical saturation at the absorption peak, which emphasizes the tails. The remaining difference between Γ_{PD} and Γ_{ATR} is attributed to the influence of the collective nature of the IS excitations on the linewidth and lineform.[24,25] In a system with nonparabolic subband structure, the PD line shape is broadened, since it is sensitive to the independent electron transitions. Γ_{ATR}, on account of the collective properties of the ISR, remains small.

In sample C, a δ doping is placed in the center of the well. The decrease in mobility from the RT (2100 cm^2/V s) to the 77 K (1500 cm^2/V s) value indicates that scattering by ionized impurities is the dominating mechanism. Since the electron wave function of the ground state has its maximum at the well center, and is therefore more affected by the δ doping, one expects the ratio R to be drastically reduced compared to the modulation-doped case discussed above. The experiment indeed confirms the predicted influence of the doping upon the ratio, which is found to be $R=0.6$ at RT. This ratio manifests itself in a sample characteristic line shape, as can be seen in Fig. 6. The estimated ratio determined by the mobility and the FT absorption linewidth ($\Gamma_{ATR}\simeq 22.4$ meV) would give an upper bound of $R\leqslant 1.4$.

We also performed experiments with samples having the δ doping at the position of the wave function maximum of the first excited subband state. A direct comparison to sample C is found to be difficult, since the doping-induced asymmetry leads to a photosignal that we relate to the build-up of a static polarization. This phenomena may be suppressed in symmetrically non-center-doped QW's.

B. Responsivity

In this section we compare the theoretical PD response quantitatively with the experimental values obtained by mea-

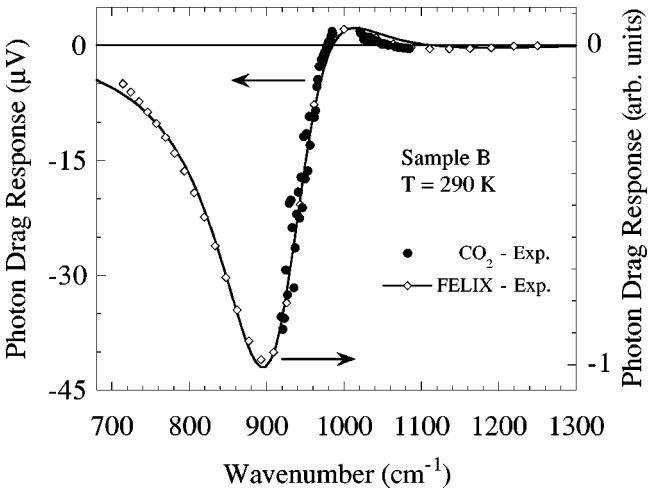

FIG. 7. PD open loop voltage (dots) over the length $l = 3.6$ mm of the active area of sample B as a function of the photon energy. A high-frequency PD measurement (open circles) was performed with FELIX to obtain the entire line shape. The intensity of the exciting CO_2 light within the sample was 6.4 W/cm^2 at 921 cm^{-1}.

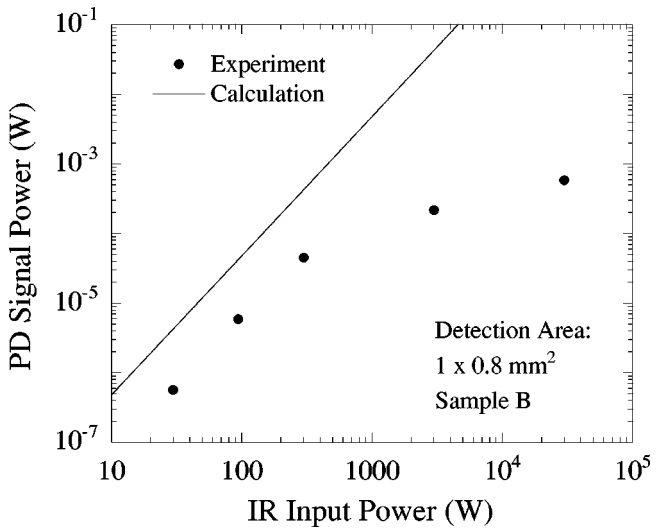

FIG. 8. A typical detector performance in terms of conversion efficiency, measured with FELIX at 11.2 μm, is plotted (dots) for comparison with the calculated upper limit (line). The difference is mainly attributed to transmission line losses. The PD signal output power has a quadratic dependence on the IR input power, and is limited by saturation at higher intensities.

suring the PD open loop voltage. In this experiment, the CW ir beam of a CO_2 laser was modulated at 2 kHz by a chopper and used as the excitation source. The standard lock-in technique was applied to obtain the PD response. By tuning the CO_2 laser over the strongest lines of its four bands, we sampled photon frequencies from 920 to 1080 cm^{-1}.

The direct contribution of the PD response can be derived from the excess velocity, $v = p/m^*$, to which an electron is excited by the absorption of a single photon with momentum p. In the exposed active area, where l and w are the length and width, respectively, the contribution of one excited electron to the current is then simply given by $i_e = -ev/l$. The steady state current due to all excited electrons is thus

$$i_s = i_e \dot{N} l w \tau_p = -e\tau_p \frac{h\nu n}{m^* c} \dot{N} w, \tag{4}$$

where τ_p is the momentum relaxation time and $\dot{N}$ is the number of excitations per unit time and area. The open loop voltage U_o of the direct PD is built up over the illuminated length with the resistance $R = l/(eN_{el}\mu_{Hall} w)$. The Hall mobility $\mu_{Hall} = e\tau_{Hall}/m^*$ [$\mu_{Hall}(300\ \text{K}) = 7200$ cm^2/V s for sample B] is related to the current relaxation time τ_{Hall}. We thus obtain

$$U_o = Ri_s = -\frac{h\nu n}{ce} l \frac{\dot{N}}{N_{el}} \frac{\tau_p}{\tau_{Hall}}. \tag{5}$$

In Fig. 7 we plot the experimentally observed PD open loop voltage (full circles) of sample B as a function of the photon energy. A high-frequency PD measurement (open circles) was performed with FELIX to obtain the entire line shape. The intensity of the exciting CO_2 light was 6.4 W/cm^2 within the sample at the photon energy of 921 cm^{-1}. The illumination was homogeneous over the active area with length $l = 3.6$ mm. To compare the experimental response with the theoretical estimation, the experimental values are separated into a direct and a resonant part according to Eq. (1), yielding a direct signal of 28 μV at 933 cm^{-1} (the absorption peak position). Assuming full absorption and $\tau_p = 0.5\tau_{Hall}$, we obtain the same value by using Eq. (5). This assumption is reasonable because the hole excitations in the PD effect cover a larger energy range ($\sim E_F$) than the thermal energy range ($\sim kT$) relevant for the equilibrium transport. Taking into account that the illuminated length and the intensity in the active layer used for the estimation are likely to be overestimated and/or that coupling losses due to an air gap between the Ge prism and the active layer may have occurred, we conclude that τ_p [corresponding to τ_2 in Eq. (1)] is even closer to τ_{Hall}.

In the following, we determine the efficiency of the PD effect when used as an ultrafast IR detector. In this case the PD response is to be understood as an ac current in a transmission line with a given impedance Z_w. In our case $Z_w = 31\ \Omega$ for $\omega \geqslant 1$ MHz. As a consequence, the output power has a quadratic dependence on the IR input power. This implies that the efficiency steadily increases with increasing power, making it favorable to operate this device at higher intensities. This advantage cannot be taken too far, since saturation occurs. The relevant parameters affecting saturation are the electron density in the QW system and the intersubband energy relaxation processes.

A typical detector performance in terms of conversion efficiency, measured with FELIX at a wavelength of 11.2 μm, is shown in Fig. 8. The 4-ps (FWHM) ir pulses illuminate the 0.8-mm-wide active microstrip mesa over a length L of 1 mm. The actual output power during the 4 ps is obtained from the measurement by assuming conservation of total energy of the electrical pulse in the transmission line. The broadening of the pulse, due to limitations in bandwidth, is thus compensated.

An estimation of the PD output power is derived by considering distributed PD current sources in the HF transmission line. The HF attenuation in the line is given by α_{el}

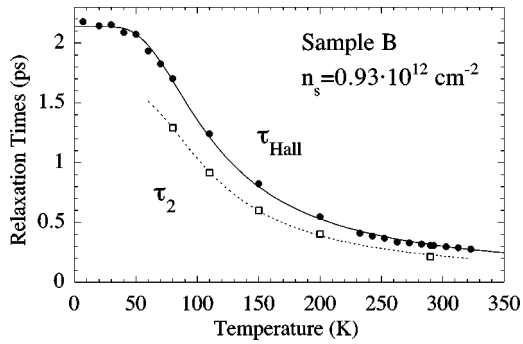

FIG. 9. Current relaxation time τ_{Hall} (dots) obtained by the Hall mobility as a function of temperature. The momentum relaxation time τ_2 (open squares) is obtained by assuming $\tau_1 \sim \tau_{Hall}$ and with help of the measured ratio R (cf. Fig. 10). The lines are guides to the eye. At high temperatures ($T>70$ K) LO-phonon scattering dominates and determines the temperature dependence.

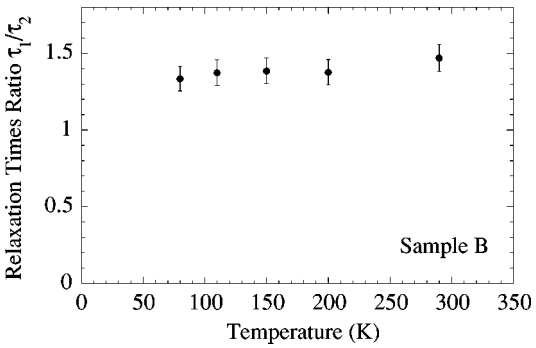

FIG. 10. Momentum relaxation time ratio $R=\tau_1/\tau_2$, extracted from the PD spectra for various temperatures. The ratio R remains approximately constant over the entire temperature range.

$=R'/(2Z_w)=(1.6\ \text{mm})^{-1}$ for sample B. The electrical pulse propagation is defined by the equivalent circuit model and by applying Kirchhoff's laws.[10] To obtain the peak signal from the entire distributed detector, we simply time integrate the distributed signals over the detector length, including dissipation effects. The result for the peak signal under the condition of velocity matching[21] between electrical and optical pulse propagation is the same as in Eq. (5) but with a prefactor of $1/(\alpha_{el}L)$. The optical absorption is 75% at 893 cm^{-1}, and the direct and resonant PD contributions are equally strong. The predicted upper limit (solid line in Fig. 8), obtained by assuming again that $\tau_2 \sim \tau_{Hall}$, is approximately a factor of 7 above the measured PD output power. Part of the difference between the calculated and the experimental results are due to transmission line losses.

C. Temperature dependence

In Fig. 9, the current relaxation time τ_{Hall} of sample B obtained by the Hall measurements is plotted versus temperature. As argued above, the equilibrium transport time τ_{Hall} at RT is a good estimate for the momentum relaxation time τ_1 of holes in the ground subband, although the holes are distributed over all possible wave vectors. We assume that $\tau_1 \sim \tau_{Hall}$ also applies at lower temperatures. The momentum relaxation time τ_2 in the second subband is then obtained with the help of the experimental relaxation time ratios, $R=\tau_1/\tau_2$, extracted from the PD spectra at the corresponding temperatures. We find for sample B that the ratio R remains almost constant over the temperature range from 80 K up to RT, with a value of ~ 1.35, as can be seen in Fig. 10.

The general trend of τ_{Hall} can be understood by considering the dominant scattering mechanisms. At low temperatures, interface roughness limits the mobility. At high temperatures ($T>70$ K), the LO-phonon scattering dominates, and the principal temperature dependence is determined by the phonon occupation number.[26] A proper theoretical treatment of the LO-phonon-limited mobility would be obtained from a solution of the appropriate Boltzmann equation.[27]

At first sight, it is surprising that the ratio R stays almost constant over the examined range. In comparison to the situation in the ground subband, we expect that in the second subband the momentum decay will be influenced by LO-phonon emission, which should therefore be less sensitive to phonon occupation and thus temperature. On the other hand, since the electron-electron interaction leads to an equilibrium between subbands on a subpicosecond time scale,[28] it may be argued that there is not much difference in the temperature-dependent probability of a carrier being initially in the second or the first subband. The constant ratio R would then be determined by subband specific scattering occurring on a subpicosecond time scale. Such a process should, according to our results, have the same temperature dependence for both subbands. More experiments are needed to clarify this issue, e.g., on the δ-doped sample C, where we would expect a temperature dependent ratio R, due to the stronger influence in the ground subband of the Coulombic impurity scattering.

In this context we would like to point out a recent publication of Faleev and Stockman,[29] who also addresses the topic of temperature-dependent PD ratios. Systems with $E_{12}<\hbar\omega_{LO}$ were considered theoretically where the spectral shape is governed mainly by the resonant part. New qualitative features were predicted, such as the reversal of the PD current with changing temperature in tailored samples with a properly chosen doping profile across the well.

D. Intensity dependence

In the experiments performed with FELIX, we use pulse energies sometimes exceeding 1 $\mu\text{J/cm}^2$, deposited within typically 2 to 4 ps. At such high intensities we expect heating of the electron gas. When the electrons are excited to the higher subband they have a nonequilibrium distribution, which rapidly thermalizes to a Fermi distribution with an electron temperature T_e. The thermalization occurs in tens of femtoseconds through electron-electron scattering,[30] in which almost no energy is transferred to the lattice. During the time span of our experiment ($\sim$ picoseconds), however, the electrons lose energy to the lattice through intra- and intersubband electron–LO-phonon interactions and reach thermal equilibrium with a part of the available phonon modes. In narrow wells, where $E_{12}>E_{LO}$, the relaxation lifetime due to electron–LO-phonon scattering is found to be of the order of 0.3 ps,[31–34] which is in good agreement with theoretical estimates.[35–37] Since the group velocity of LO phonons is very small (less than 10 m/s), the phonons cannot drift away from the excitation volume during their lifetime. Instead, the LO phonons will decay into other lattice modes. The dominant process in this case is the decay of LO

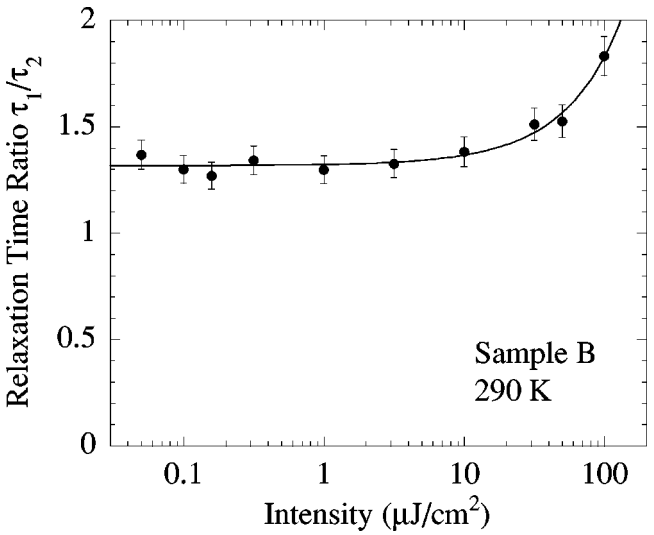

FIG. 11. Momentum relaxation time ratio $R=\tau_1/\tau_2$, extracted from the PD spectra for various intensities at RT. A constant mean energy, $\langle E(T=290\ \mathrm{K})\rangle=34.5$ meV, over the entire range is used. The line is a guide to the eye.

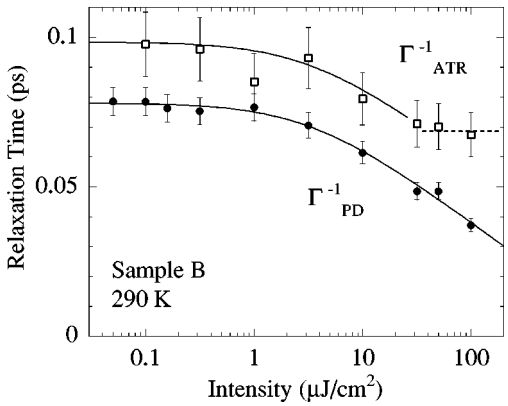

FIG. 12. Lifetimes obtained from the experimental PD linewidth Γ_{PD}^{-1} (dots), together with the lifetime Γ_{ATR}^{-1} from ATR measurements with FELIX (open squares). The lines are guides to the eye.

phonons into two longitudinal acoustic phonons. The lifetime of LO phonons at RT is typically[38] 4 ps for GaAs at 300 K. During these 4 ps, the energy of the absorbed photons is thus mainly stored in the relevant LO phonons of the GaAs QW's; the energy stored in the electron gas is very small.

For an estimation of T_e in our experiment, we begin with the specific heat $c_v\approx 0.4\ \mathrm{J\,K^{-1}cm^{-3}}$ of LO phonons derived by the dispersionless Einstein model for bulk GaAs modes. In the plane, only modes with wave vectors up to $\sim 2k_F \approx 4.7\times 10^6\ \mathrm{cm}^{-1}$ can interact, corresponding to a small part of only $\sim 8.4\%$ of the Brillouin zone boundary, which makes $\sim 0.7\%$ of the total Brillouin zone. In the experiment presented in Fig. 5, the energy of 12 μJ/cm^2 impinges on a slab consisting of 30 QW's of 82 Å, leading to an estimated increase of T_e by ≈ 170 K, after reaching an equilibrium with the coupled LO-phonon modes.[39]

In Fig. 11 we have plotted the ratio R of the momentum relaxation times as a function of ir intensity, obtained from a PD spectra series at RT, applying Eq. (1) with a constant mean energy $\langle E\rangle_{290\,\mathrm{K}}$. The relation between τ_1 and τ_2 stays approximately constant up to 10 μJ/cm^2, and then the ratio begins to increase.

At high intensities, heating of the electron system occurs. The fast electron-electron interaction drives both subbands rapidly towards a single quasiequilibrium distribution with a common electron temperature T_e, after the pulse is over.

Let us have a closer look at the situation at high intensities. If we postulate that the ratio stays constant at all intensities, then $\langle E(T)\rangle$ must vary instead. In this case, the variation can be described by an increase of temperature related to the energy pumped into the system. We determine this temperature for the case depicted in Fig. 11: At the saturation intensity[40] $I_s=60$ μJ/cm^2 we find $R=1.65$ with $\langle E\rangle_{290\,\mathrm{K}}=34.5$ meV, which has to be substituted by the appropriate energy to obtain $R=1.3$. The mean energy is then according to the second term in Eq. (1) given by

$$\langle E(T_e)\rangle=\frac{0.65}{0.3}\langle E\rangle_{290\,\mathrm{K}}=75\ \mathrm{meV}. \tag{6}$$

This mean energy is reached at $T_e=780$ K, obtained from solving Eqs. (2a)–(2c) iteratively.

An estimation of the electron gas heating was already given in Sec. IV A. Following the same arguments, one obtains at I_s an increase of the temperature by ~ 810 K, implying $T_e\approx 1100$ K. A value close to this is found by West and Roberts,[41] who determine for an IST resonant at 10.6 μm an electron temperature $T_e=1235$ K, attained per definition at the saturation intensity. The discrepancy between these much higher temperatures compared to the 780 K from Eq. (6) suggests that the ratio in fact decreases with increasing intensity, implying that the difference between τ_1 and τ_2 becomes smaller.

In Fig. 12, we show the inverse PD (Γ_{PD}^{-1}) and optical (Γ_{ATR}^{-1}) linewidth as a function of intensity for the measurement series of Fig. 11. Apparent is the difference of the relaxation times, which is due to the fact that the PD effect is related to the single-particle excitations and the ISR is a collective effect. Unexpected is the onset of the broadening already at low intensities far below saturation. Likewise unforeseen is the ATR resonance position shift at low intensities shown in Ref. 15. At high intensities close and above saturation the difference between the PD and ATR lifetimes increases. While Γ_{PD}^{-1} continues its trend towards shorter times, Γ_{ATR}^{-1} seems to level off. The heating of the system in this regime leads to an electron distribution expanding towards higher $\mathbf{k}$ in the ground subband and thus results in a broadening of the PD due to nonparabolicity. This effect does not affect Γ_{ATR}^{-1}.[25]

V. SUMMARY

To summarize, we have used the particular features of PD spectroscopy to investigate current relaxation processes in a 2DEG. The momentum relaxation time ratio $R=\tau_1/\tau_2$ of the carriers in the occupied and the first unoccupied subbands is determined from the spectral dependence of the photon drag current. A spectral line-shape comparison is made between the modulation-doped and the δ-doped samples. While R is found to be between 1.3 and 1.6 for the modulation-doped case, which indicates that the momentum relaxation time in the excited subband is shorter than in the ground subband,

we meet the reversed situation in the δ-doped sample ($R \approx 0.6$), due to the strong overlap of the scattering centers with the ground subband wave function.

The quantitative comparison of the experimental and theoretical PD response in modulation-doped QW's confirms that $\tau_2 \leqslant \tau_1 \lesssim \tau_{Hall}$. In addition to the CW sensitivity measurement with a CO_2 laser, a HF detector performance is given, where transmission line losses and the saturation constitute the main limitations.

The persistently constant ratio of $R \approx 1.3$ over the investigated temperature range is explained by the fast thermalization of the electron gas among both subbands due to electron-electron interaction, which proceeds much faster than the optical-phonon-induced intersubband relaxation. The difference between the momentum relaxation times is thus determined by subband specific processes, which take place on a subpicosecond time scale but have no temperature dependence.

The increase of the ratio from 1.3 to 1.65 when the intensity is raised to 60 $\mu J/cm^2$ (saturation intensity) could be explained by a corresponding increase in the electron temperature T_e to 780 K under the assumption that the ratio R stays constant. Since 780 K is considerably less than the estimate of 1100 K that is derived from the energy balance between the deposited laser power and the stored energy in the electron and the LO-phonon systems, we conclude that the difference between τ_1 and τ_2 decreases with increasing intensity.

We have commented on the difference between Γ_{ATR}^{-1} and Γ_{PD}^{-1}. The main deviation is attributed to collective effects affecting the underlying experiments differently. The broadening of Γ_{PD} at high intensities is explained by an occupation of higher **k** states and the related energy dispersion due to nonparabolicity.

ACKNOWLEDGMENTS

We would like to thank U. Gennser and M. Załużny for helpful discussions and B. Patterson for comments on our manuscript. We gratefully acknowledge the support by the FOM Institute in providing the required beam time on FELIX, and we highly appreciate the assistance by the FELIX staff, in particular Dr. A.F.G. van der Meer. We thank H. Siegwart (PSI) for the careful sample preparation. Part of the work was supported by the SNF.

[1] A.F. Gibson, M.F. Kimmit, and A.C. Walker, Appl. Phys. Lett. **17**, 75 (1970).
[2] A.M. Danishevskii, A.A. Kastalskii, S.M. Ryvkin, and I.D. Yaroshetskii, Zh. Éksp. Teor. Fiz. **58**, 544 (1970) [Sov. Phys. JETP **31**, 292 (1979)].
[3] L.C. West and S.J. Eglash, Appl. Phys. Lett. **46**, 1156 (1985).
[4] S. Luryi, Phys. Rev. Lett. **58**, 2263 (1987).
[5] A.A. Grinberg and S. Luryi, Phys. Rev. B **38**, 87 (1988).
[6] A.D. Wieck, H. Sigg, and K. Ploog, Phys. Rev. Lett. **64**, 463 (1990).
[7] F.K. Gel'mukhanov, J.E.M. Haverkort, S.W.M. Borst, and J. Woerdman, Phys. Rev. A **36**, 164 (1987).
[8] M.I. Stockman, L.N. Pandey, and T.F. George, Phys. Rev. Lett. **65**, 3433 (1990).
[9] H. Sigg, M.H. Kwakernaak, B. Margotte, D. Erni, P. van Son, and K. Köhler, Appl. Phys. Lett. **67**, 2827 (1995).
[10] H. Sigg, S. Graf, M. Kwakernaak, B. Margotte, D. Erni, P. van Son, and K. Köhler, Superlattices Microstruct. **19**, 105 (1996).
[11] H. Sigg, P. van Son, and K. Köhler, Surf. Sci. **361/362**, 468 (1996).
[12] For a review see Ole Keller, Phys. Rep. **268**, 85 (1996).
[13] M. Załużny, Solid State Commun. **103**, 435 (1997).
[14] X. Chen and O. Keller, Phys. Rev. B **55**, 15 706 (1997).
[15] S. Graf, H. Sigg, K. Köhler, and W. Bächtold, Phys. Rev. Lett. **84**, 2686 (2000).
[16] The depolarization shift can simply be explained by the fact that every electron feels an electric field that is dynamically screened by the polarization of all electrons.
[17] H. Sigg, in *Intersubband Transitions in Quantum Wells*, NATO ASI Series B, edited by E. Rosencher, B. Vinter, and B. Levine (Plenum Press, New York, 1992), Vol. 288, p. 83.
[18] The transfer matrix method is employed, where the MQW system is characterized as a whole by a complex effective medium dielectric function ε_{QW}. The intersubband absorption strength, and thus ε_{QW}, is calculated in the dipole approximation applying Fermi's golden rule.
[19] M. Załużny and C. Nalewajko, Phys. Rev. B **59**, 13 043 (1999).
[20] F. Capasso, C. Sirtori, D. Sivco, and A.Y. Cho, in *Intersubband Transitions in Quantum Wells*, NATO ASI Series B, edited by E. Rosencher, B. Vinter, and B. Levine (Plenum Press, New York, 1992), Vol. 288, p. 141.
[21] M.H. Kwakernaak, D. Erni, and H. Sigg, in *New Directions in Terahertz Technology*, NATO ASI Series E, edited by J.M. Chamberlain and R.E. Miles (Kluwer Academic, Dordrecht, 1997), Vol. 334, p.143.
[22] F. Keilmann, Solid State Commun. **92**, 223 (1994).
[23] D. Oepts, A.F.G. van der Meer, and P.W. Amersfoort, Infrared Phys. Technol. **36**, 297 (1995).
[24] T. Ando, A.B. Fowler, and F. Stern, Rev. Mod. Phys. **54**, 437 (1982).
[25] R.J. Warburton, K. Weilhammer, J.P. Kotthaus, M. Thomas, and H. Kroemer, Phys. Rev. Lett. **80**, 2185 (1998).
[26] K. Hess, Appl. Phys. Lett. **35**, 484 (1979).
[27] J.B. Roy, P.K. Basu, and B.R. Nag, Solid State Commun. **40**, 491 (1981).
[28] M. Hartig, S. Haacke, P.E. Selbmann, and B. Deveaud, Phys. Rev. Lett. **80**, 1940 (1998).
[29] S.V. Faleev and M.I. Stockman, Phys. Rev. B **59**, 7338 (1999).
[30] T. Elsaesser, J. Shah, L. Rota, and P. Lugli, Phys. Rev. Lett. **66**, 1757 (1991).
[31] F.H. Julien, J.M. Lourtioz, N. Herschkorn, D. Delacourt, J.P. Pocholle, M. Papuchon, R. Planel, and G. Le Roux, Appl. Phys. Lett. **53**, 116 (1988); **62**, 2289 (1993).
[32] M.C. Tatham, J.F. Ryan, and C.T. Foxon, Phys. Rev. Lett. **63**, 1637 (1989).
[33] D. Cui, Z. Chen, S. Pan, H. Lu, and G. Yang, Phys. Rev. B **47**, 6755 (1993).

[34] J. Faist, F. Capasso, C. Sirtori, D.L. Sivco, A.L. Hutchinson, S.N.G. Chu, and A.Y. Cho, Appl. Phys. Lett. **63**, 1354 (1993).
[35] B.K. Ridley, Phys. Rev. B **39**, 5282 (1989).
[36] J.K. Jain and S. Das Sarma, Phys. Rev. Lett. **62**, 2305 (1989).
[37] H. Rücker, E. Molinari, and P. Lugli, Phys. Rev. B **44**, 3463 (1991).
[38] D. von der Linde, J. Kuhl, and H. Klingenberger, Phys. Rev. Lett. **44**, 1505 (1980).
[39] This estimation is in good agreement with a calorimetric measurement using in-plane photoconduction.
[40] The saturation intensity is defined as the intensity required to lower the absorption by a factor of 2.
[41] L.C. West and C.W. Roberts, in *Quantum Well Intersubband Transition Physics and Devices*, NATO ASI Series E, edited by H.C. Liu, B.F. Levine, and J.Y. Andersson (Kluwer Academic, Dordrecht, 1994), Vol. 270, p. 501.